A new active power controller in dual active bridge DC-DC converter with a minimum-current-point-tracking technique.

HEBALA, O.M., ABOUSHADY, A.A., AHMED, K.H., ABDELSALAM, I. and BURGESS, S.J.

2021

A New Active Power Controller in Dual Active Bridge DC-DC Converter with a Minimum-Current-Point-Tracking Technique

Osama M. Hebala, Ahmed A. Aboushady, *Senior Member*, *IEEE*, Khaled H. Ahmed, *Senior Member*, *IEEE*, Ibrahim Abdelsalam, Samuel J. Burgess

***Abstract*— This paper proposes a new controller for power regulation in dual active bridge (DAB) DC−DC converter based on a new scheme that tracks minimum RMS current to ensure minimum losses. The proposed controller is based on an implementation of perturb and observe (P&O) tracking method that enables minimum current point tracking (MCPT) at any desired level of active power transfer and DC voltage ratio. The P&O is embedded in a closed loop control scheme which simultaneously regulates active power in DAB converter. The non-linear I-V characteristic of DAB presents the basis for this proposed controller and the rationale of using P&O algorithm. The proposed controller does not require complex non-linear converter modelling and is not circuit parameter dependent. Design procedure of the proposed controller is presented, and extensive simulation is carried out using MATLAB/Simulink to validate effectiveness of the proposed MCPT closed loop controller. An experimental prototype also substantiates the results achieved.**

***Index Terms*—Dual Active Bridge (DAB), Minimum Current Point Tracking (MCPT), Perturb and Observe (P&O), RMS Current stress.**

I. INTRODUCTION

DUAL active bridge (DAB) DC−DC converters have attracted significant attention in various fields, such as: high voltage DC (HVDC) transmission systems, medium voltage DC (MVDC) as well as DC microgrids applications [1–3]. This is mainly due to several key advantages offered by DAB converters such as zero voltage switching (ZVS) characteristics, high power density, high power handling capability, cascaded or modular configuration capability (in the case of higher power/voltage requirements) and galvanic isolation in transformer based versions [4]–[6]. This clarifies the existing trend toward the performance improvement - thus minimisation of losses - in DAB DC−DC converter.

There are different technical aspects considering the minimisation of DAB losses: particularly, the minimisation of non-active power losses [7]–[9] and current stresses [10]–[15]. In [7] high DAB performance was investigated by obtaining an operating range of optimum triple phase shift (TPS) ratios via analyzing the inductor current for light and heavy loads in boost operation. However, the work was based on the extended phase shift (EPS) control resulting in sub-optimal operating points at light loads. Authors in [8] proposed a neural-network-based controller that was designed using a non-generalised per unit analysis which does not incorporate buck and boost resulting in rating-specific analysis. Reactive power minimisation was tackled in [9] using particle swarm optimisation (PSO) considering a harmonics-based DAB model that is limited up to the 7th harmonic. In [14], a numerical optimized method employing a hybrid phase shift technique was developed to achieve minimum inductor RMS current at a specific power transferred. However, both [9] and [14] utilised look-up tables which involve difficulties in practical implementation as for every run of the test rig, the implemented DSP needs to be loaded with the look up table at the initialization. In addition, the universality is overlooked as large amount of offline case-specific calculations – that are dependent on DC voltage ratio and power levels – are needed. The proposed converter switching modes in [12] do not entirely cover the bidirectional power range which jeopardizes the correctness of the derived controller. In addition, peak inductor current was used as the minimisation objective however the major DAB loss is the conduction loss which is related to the RMS current [16]. There are also hardware methods implemented for efficiency improvements in DAB converters such as the utilisation of GaN and SiC switch devices. In this context, [17] utilised GaN in modified DAB-based topology. However, the scope of this paper is on control design not device level performance.

This Manuscript received February 5, 2020; revised March 13, 2020 and May 30, 2020; accepted July 22, 2020. Date of publication ……; date of current version …….. *(Corresponding author: Osama Mohamed Hebala.)*

O. M. Hebala is with Electric and Control Engineering Department, Arab Academy for Science and Technology and Maritime Transport, Alexandria 1029, Egypt (e-mail: ohibala@aast.edu).

A. A. Aboushady is with the School of Computing, Engineering and Built Environment, Glasgow Caledonian University, Glasgow G4 0BA, U.K (e-mail: ahmed.aboushady@ieee.org).

K. H. Ahmed is with the Department of Electronic and Electrical Engineering, University of Strathclyde, Glasgow G1 1XW, U.K, and the Department of Electrical Engineering, Faculty of Engineering, Alexandria University, Alexandria, Egypt (e-mail: khaled.ahmed@ieee.org).

I. Abdelsalam is with the Electrical Engineering Department, Arab Academy for Science and Technology and Maritime Transport, Alexandria 1029, Egypt (e-mail: i.abdelsalam@aast.edu).

S. J. Burgess is with the School of Engineering, Robert Gordon University, Aberdeen AB10 7AQ, UK (e-mail: s.j.burgess@rgu.ac.uk).

Color versions of one or more of the figures in this paper are available online at http://ieeexplore.ieee.org.

.

The reported literature in the area of efficiency-improving control schemes of DAB show various shortcomings that can be summarised as follows:

a) Dependency of the control design on complex TPS-based time-domain modelling such as [6]–[15]. In this case, detailed operation modes and related boundaries under different conditions in terms of load and DC voltage ratio must be determined which complicates control schemes design.
b) Non universal control design that require offline calculation, pre-set values or look up tables for implementation which is computationally exhaustive and requires complex inter/extrapolation, such as the work in [9] and [14].
c) Sub-optimal TPS solutions due to:
   - Using control scheme derived from approximate harmonics-based modelling (i.e.: ignoring the effect of higher order harmonics on RMS current.), such as the work in [9].
   - Restricting optimisation to a specific control technique (i.e.: using EPS [7] and/or dual phase shift [13] thus not utilising all possible degrees of freedom in phase shift control.). This leads to high current stresses and circulating conduction loss under light load and/or unmatched voltage amplitudes across the AC link (transformer) sides (i.e.: unequal DC voltage levels.).
   - Using optimization methods that lack sufficiency due to the non-convex feasible region of the DAB optimization problem. For example, Lagrange multiplier (LMM) method were used in [11] & [12] to minimise DAB current stress. In addition, it is too complicated to use Karush-Kahn-Tucker (KKT) conditions for minimizing current and determining the ZVS boundary conditions (as was used in [11]) because four order algebraic equations must be solved.

This underpins the need for further advancements in the area of control scheme design and optimization in DAB converters. To date, no work has proposed a universal solution for DAB converter that tackles the aforementioned issues without compromising on control complexity and challenging real time implementation. On this basis, the work discussed here proposes a control scheme for active power regulation that can always track minimum current in DAB converter for any desired power transfer level. In addition, this paper considers a generic use case, which includes two fixed or variable DC side voltages (e.g. batteries or controlled DC busses in a DC grid). Moreover, the proposed control scheme is based on a new adaptation of P&O methods, such as those in MPPT algorithms [18]–[22]. P&O algorithms are simple in terms of implementation and do not require prior knowledge of the converter characteristics. In relation to the perturb calculation, there are basically two types: fixed-step perturb [18]–[20] and adaptive-step perturb [21], [22]. Adaptive-step P&O is investigated in this paper given that fixed-step perturb suffers from several demerits in steady state and the perturb value is not generic. The new developed adaptive-step perturb and observe utilises the converter's AC link RMS current rate of change by implementing a simple PI controller to generate an adaptive perturb to the bridges' duty ratios. Advantages of the proposed technique are as follows:

a) Precise power flow regulation;
b) AC link RMS current minimization;
c) Universal controller design that includes the effect of DC voltage ratio, is not rating-specific and is not dependent on complex non-linear modelling;
d) Low computational burden required and simple to implement as only PI controllers are needed;
e) No oscillation in steady state operations as the adaptive algorithm automatically generates variable perturb.

In this paper, section II covers the development of I-V DAB characteristic plane that provides the grounds for the proposed P&O minimum current point tracking (MCPT) algorithm. Section III demonstrates the adaptation of P&O for DAB converters and embedding of P&O algorithm in the power flow controller. The closed loop controller design is then provided in section IV. Extensive simulation and experimental results are presented in sections V and VI respectively. Section VII concludes the paper.

II. Non-linear DAB Characteristics

A. Phase Shift Modulation

The switching model of the DAB converter is indicated in Fig. 1. The power flow between any two ports is essentially controlled through phase shift modulation of the square-wave voltages generated by their corresponding active bridge modules.

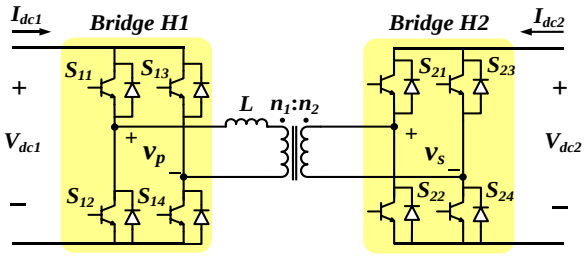

Fig. 1. DAB DC-DC converter.

The modulation scheme adopted is the triple phase shift (TPS) [15] depicted in Fig. 2. The degrees of freedom available are the bridge voltages duty ratios D_1 and D_2 respectively and phase shift D_{12}. These control parameters are obtained using classical phase shifting of gate signals S_{11}-S_{14} and S_{21}-S_{24} as shown in Fig. 2(a). Modulation parameters (D_1, D_2, D_{12}) are normalised with respect to half the switching cycle (T_h) such that the equivalent per unit ranges are $0 \leq D_i \leq 1$ and $-1 \leq D_{12} \leq 1$. The representation of the DAB AC voltage and current waveforms are shown in Fig.2(b). where K_{12} represents the DC voltage ratio as outlined by (1). The inclusion of this ratio enables representation of DAB's different operating modes, such that K_{12}=1 designates unity-gain mode and $K_{12}\neq 1$ designates buck/boost mode. The instantaneous AC side current can be derived from (2).

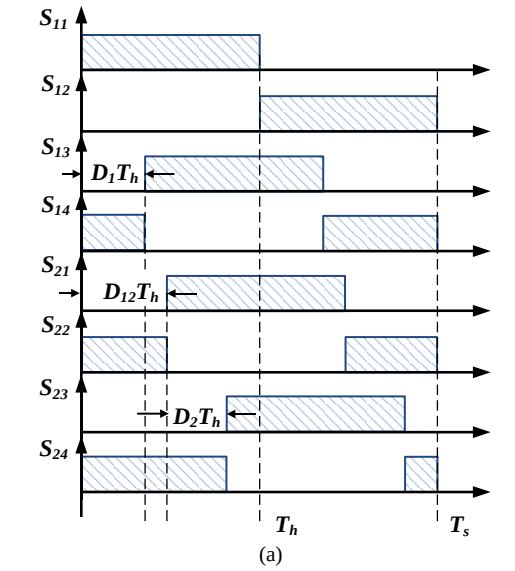

(a)

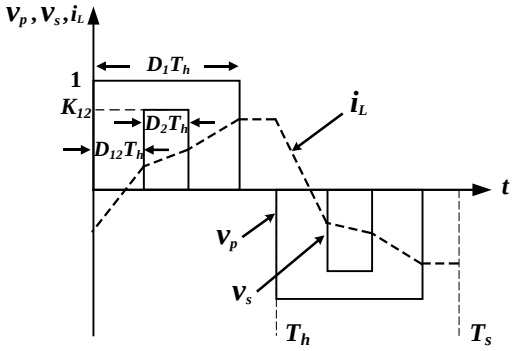

(b)

Fig. 2: Triple phase shift control in DAB. (a) switching signals, (b) definition of key waveforms.

$$K_{12} = \frac{n_1 V_{dc2}}{n_2 V_{dc1}} \tag{1}$$

Where,
- n_1, n_2 are turns number for transformer's primary and secondary sides
- V_{dc1}, V_{dc2} are DC sides voltages

$$i_L(t) = \frac{1}{L}\int_{t_n}^{t} \left(v_p(t) - v'_s(t)\right) dt + i_L(t_n) \tag{2}$$

Where
- $v_p(t)$ is primary voltage
- $v'_s(t)$ is secondary voltage refereed to primary
- L is equivalent inductance
- t_n represents n^{th} switching instant.

B. I-V Characteristic

The objective in this section is to define the DAB AC current characteristics with respect to the bridge voltages. Assuming non-isolated lossless DAB, the independent variables of the proposed I−V DAB characteristic are the RMS bridge voltages $V_{p_{RMS}}$, and $V_{s_{RMS}}$ given by (3) in per unit form to provide standardized analysis (base voltage V_{base}=V_{dc1}). On the other hand, the dependent variable is the AC link's RMS current $I_{L\,RMS}$ outlined by (4) which is function of the DC voltage ratio K_{12} in addition to the triple phase shift parameters D_1, D_2 *and* D_{12} [15].

$$V_{p_{RMS(pu)}} = \sqrt{D_1},\ V_{s\,RMS(pu)} = K_{12}\sqrt{D_2} \tag{3}$$

$$I_{L\,RMS}{}^2(K_{12}, D_1, D_2, D_{12}) = \frac{1}{T_h}\int_0^{T_h} i_L{}^2(t)\ dt. \tag{4}$$

For the ease of analysis, full range of a single independent variable $V_{p_{RMS}}$ is plotted against the dependent variable $I_{L\,RMS}$ at certain operating point (P=*0.25pu and* K_{12}=*0.5*). The output is multiple 2D I-V curves between $I_{L_{RMS}}$ and $V_{p_{RMS}}$ for several discrete values of $V_{S_{RMS}}$. This is shown in Fig.3(a), where the nonlinear I-V characteristic is clearly presented. It is also noted that some points in the curves are empty, which means that the relevant RMS voltages (i.e.: TPS ratios D_1, D_2 *and* D_{12}.) do not achieve reference power P=0.25pu. To better show the I-V characteristic at full range of the independent variables ($V_{p_{RMS}}$ and $V_{s_{RMS}}$), a 3-D representation is developed as shown in Fig.3 (b), where $V_{p_{RMS}}$ and $V_{s_{RMS}}$ are plotted along the horizontal axes, and $I_{L_{RMS}}$ is plotted along the vertical axis at the same operating point (P=*0.25pu and* K_{12}=*0.5*). Note that per unit power is calculated based on V_{base}=V_{dc1} and Z_{base}=$8f_sL$ [15] where f_s=$1/T_s$.

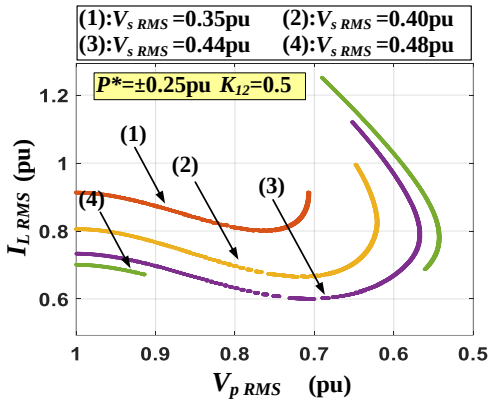

(a)

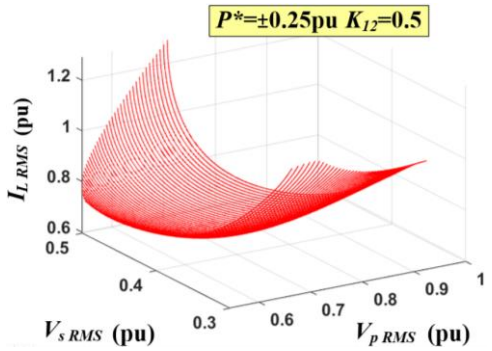

(b)

Fig.3: Representation of DAB I−V Characteristic Plane at single operating point P*=0.25pu and K_{12}=0.5- (a) 2D at multiple discrete values of V_{sRMS}. (b) 3-D Representation at full range of V_{sRMS} and V_{pRMS}.

The I−V DAB characteristic plane generically applies to any DAB and shows that there is only one specific combination of bridge voltages (at each level of power) that gives the global minimum current. From (3), $V_{p_{RMS}}$ and $V_{s_{RMS}}$ are solely dependent on D_1 and D_2 respectively, therefore the minimum current point can be achieved by a unique combination of D_1 and D_2 at a specific power. The remaining degree of freedom is the phase shift angle D_{12} which will be regulated via a PI controller to realise power flow control. Consequently, the main challenge is how to obtain a unique global optimal combination of duty ratios (D_1, D_2) which, in turn, regulates the RMS bridge voltages in order to track minimum current point.

III. Adaptation of P&O for DAB Converter

The search for minimum RMS current point in the universal I-V characteristic follows what can be described as a 'hill-descent' fashion with the starting point of this hill being at maximum RMS bridge voltages. Similar to the hill-climb P&O based MPPT algorithm [22], the proposed 'hill-descent' P&O-based MCPT is investigated in this section on the following basis:

- Perturbing a specific control parameter, i.e.: increasing or decreasing by a certain amount (step size);
- Measuring the AC link's RMS current and active power transferred between the two DC sides before and after the perturbation;
- The algorithm should then either: continue to perturb the system in the same direction, or perturb in the reverse direction until minimum current point (MCP) is reached.

A. *Perturbation Parameter*

Development of the hill-descent P&O MCPT technique requires primarily identification of the main perturbation parameter. Since, the objective of the P&O is to track minimum RMS current, therefore, the perturbation parameter has to be restricted to D_1 or D_2, as the analysis in section II-B has revealed. Selecting D_1 as the P&O perturbation parameter, a mathematical relationship can be derived for its corresponding value of D_2 that would ensure minimum current. This is done by equating the two RMS bridge voltages in (3) based on RMS voltage of the quasi-square waves in Fig.2. Equating the two voltages in (3) gives the direct relationship, between the duty ratios

$$D_2 = \begin{cases} \dfrac{D_1}{{K_{12}}^2} \\ 1, \quad if \ \dfrac{D_1}{{K_{12}}^2} > 1 \end{cases} \tag{5}$$

Therefore, perturbing D_1 while maintaining the relation in (5) to calculate D_2 will lead to the MCP. Investigation of D_1 as a perturbation parameter is provided here to verify the effectiveness of perturbing D_1 on RMS current. A simulation is carried out according to the following steps:

1) D_1 =1 (maximum bridge 1 voltage corresponding to top of hill in Fig.3).
2) Calculate D_2 using (5).
3) For given P and K_{12}, use (4) to calculate AC link RMS current.
4) Calculate new value of D_1 (D_1=$D_{1\text{old}}$−ΔD_1), where ΔD_1 is a fixed-step perturb.
5) Repeat steps 2-4 and stop when MCP is reached.

Fig. 4 (a),(b) shows the simulation results where RMS current follows a 'hill-descent' profile when perturbing D_1. Results also prove that perturbing D_1 leads to minimum current point MCP while maintaining the desired power at the constant required rate during the perturbation process. Accordingly, D_1 will be utilised as the perturbation parameter. The general Hill-descent RMS current profile of DAB converter under perturbation (at any operating point P* & K_{12}) is shown Fig.4(c). The perturbation starts from the left at D_1=1 and D_2=1 as these are maximum duty ratios (i.e.: corresponding to maximum RMS bridge voltages), therefore can be a valid point to initiate the search (search for minimum current point) regardless of the reference power level. To draw Fig.4(c), fixed perturbation (for the sake of simplicity) is applied on D_1 and value of D_2 is calculated via (5). Accordingly, the current starts to decrease until it reaches minimum current point (MCP) at optimal (unique) combination of $(D_1)_{\text{opt}}$ and $(D_2)_{\text{opt}}$. Phase shift D_{12} is regulated to track the desired transferred power P*.

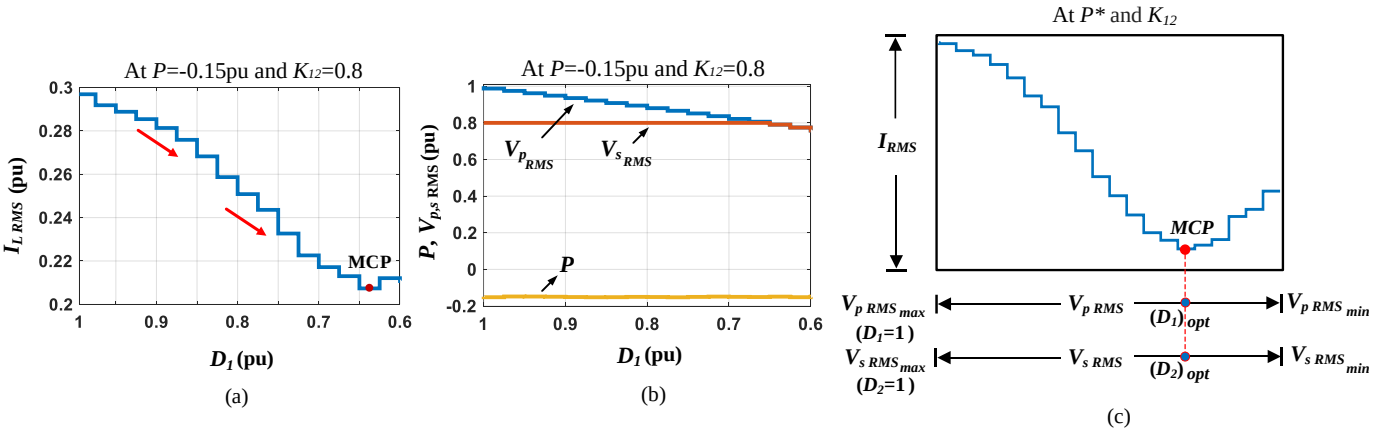

Fig. 4: D_1 Perturbation on DAB with K_{12} = 0.8 at P*=-0.15pu. (a) RMS current (b) RMS AC link voltages. (c) General representation of Hill-descent RMS current profile under Perturbation at operating point P* & K_{12}.

B. Perturb Calculation Method

This section's objective is to design an adaptive-step perturb calculator for DAB converter. The main requirement of the adaptive-step perturb is to produce large perturb steps at the start of the hill-descent technique to help reach the minimum current point (MCP) quickly, and as the MCP is approached, reduced perturb step sizes are utilised to avoid large oscillations around this MCP in steady state. In addition, an adaptive perturbation has to be generated according to the system variation. On this basis, this paper proposes a dual-component adaptive-step perturb such that the adaptive perturbs are added or subtracted from the past duty ratio D_1 based on the transferred power and AC link RMS current variations. Accordingly, a PI-based adaptive-step perturb calculator is developed as indicated by Fig. 5.

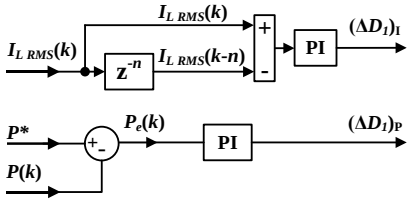

Fig. 5: Dual component PI-based adaptive-step perturb calculator.

The first adaptive component $(\Delta D_1)_I$ is to be calculated as a function of the change in RMS current after and before perturbation. $(\Delta D_1)_I$ will tune the perturbation parameter, D_1, in order to track minimum current. This is done by treating this value (i.e.: change in RMS current.) as an error signal that needs to be minimized at steady state in a closed loop system with the aid of a conventional PI controller [22]. The change in the AC link's RMS current is defined as the difference between two successive samples calculated within a fixed delay (T_d) of (n) sampling instants such that $T_d=n/f_{samp}$ where f_{samp} is the sampling frequency. This delay allows $I_{L\,RMS}$ to reach steady state after updating of modulation parameters, and is arbitrary. Furthermore, since active power regulation is the primary objective concerning the proposed controller, then the power transfer needs monitoring during the D_1 perturbation to ensure P remains regulated. This is where the second adaptive component $(\Delta D_1)_P$ is brought into play to update D_1 with respect to the measured transferred power (P) as depicted in Fig.6. The error between the measured/actual power transfer and the reference power level, defined as $P_e=|P^*-P|$, will be handled after every perturbation by a PI controller in order to generate an adaptive perturb $(\Delta D_1)_P$ that maintains this error close to zero during D_1 perturbation. This will help to decouple the impact of perturbation to D_1 from the main closed loop active power regulation controller, which will be discussed in section IV. The weights of the two perturb components are arbitrary, however, since current minimization totally depends on the P&O algorithm, the weight of $(\Delta D_1)_I$ should be higher than $(\Delta D_1)_P$. Especially that the main function of $(\Delta D_1)_P$ is only to finetune D_1 given that a separate controller is utilised for power regulation. Accordingly the recommended limits for the perturb components are $0\leq(\Delta D_1)_I\leq 0.2$pu and $0\leq(\Delta D_1)_P\leq 0.1$pu. Functions of the proposed dual-component adaptive-step PI-based perturbs can therefore be summarised as follows:

- **$(\Delta D_1)_I$**: an adaptive perturb needed to update D_1 with respect to the RMS current response depending on the incremental or decremental change of $I_{L\,RMS}$ then $(\Delta D_1)_I$ is generated to update (correct) the value of D_1.
- **$(\Delta D_1)_P$**: an adaptive perturb needed to fine tune D_1 to ensure error in active power is maintained close to zero during the D_1 perturbation process to decouple this from main active power regulation controller.

C. Hill-Descent P&O Algorithm

The proposed P&O algorithm perturbs D_1 (starting at max D_1=1) while observing variation of $I_{L\,RMS}$ and P_e. There are eight operating conditions, outlined in Table I, taking into consideration that sign of $(\Delta D_1)_I$ depends on whether the change in RMS current is positive or negative, i.e. increase in RMS current means positive $(\Delta D_1)_I$ and decrease in RMS current means negative $(\Delta D_1)_I$. There is redundancy within these eight conditions, thus they can be reduced into only four conditions given by (6). On this basis, the full proposed hill-descent P&O algorithm is depicted in Fig.6. A small tolerance in power error (P_{Tol}=0.005pu) is used to indicate accepted power error, as zero tolerance can lead to sub-optimal solutions. The implementation steps of the proposed hill-descent P&O algorithm are as follows:

a) Read the signals of AC link's RMS current $I_{L\,RMS}$(k) and power transfer $P(k)$ where k refers to the present sampling instant;
b) Calculate adaptive perturb values $(\Delta D_1)_I$ and $(\Delta D_1)_P$.
c) $(\Delta D_1)_I$, $(\Delta D_1)_P$ and $P_e(k)$ are sent to P&O algorithm which determines $D_1(k)$ while $D_2(k)$ is calculated using (5).
d) Updated and previous values ($D_1(k\text{-}1)$ and $D_1(k\text{-}n)$) are sent back to the P&O for next iteration.
e) Repeat steps (a)-(d).

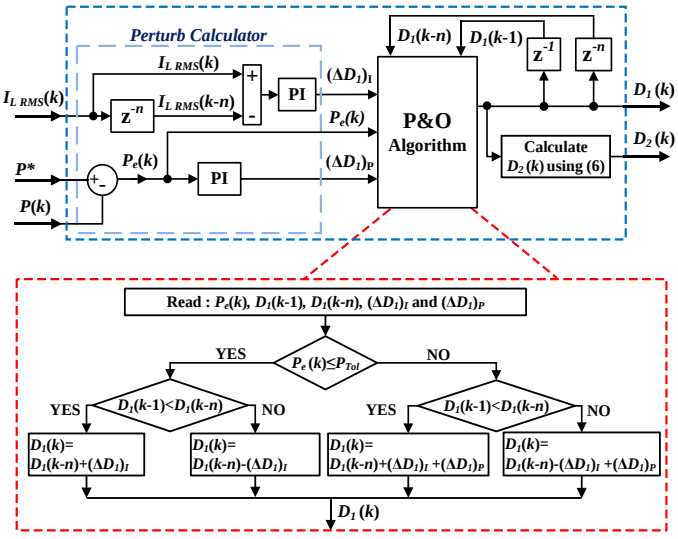

Fig. 6: MCPT Technique composed of the Hill-Descent Perturb and Observe algorithm and the dual component PI-based adaptive-step perturb calculator.

$$D_1(k)=\begin{cases} D_1(k-n)+(\Delta D_1)_I, & [P_e(k)\leq P_{Tol}\ \text{AND}\ D_1(k-1)<D_1(k-n)] \\ D_1(k-n)-(\Delta D_1)_I, & [P_e(k)\leq P_{Tol}\ \text{AND}\ D_1(k-1)>D_1(k-n)] \\ D_1(k-n)+(\Delta D_1)_I+(\Delta D_1)_P, & [P_e(k)>P_{Tol}\ \text{AND}\ D_1(k-1)<D_1(k-n)] \\ D_1(k-n)-(\Delta D_1)_I+(\Delta D_1)_P, & [P_e(k)>P_{Tol}\ \text{AND}\ D_1(k-1)>D_1(k-n)] \end{cases} \quad (6)$$

TABLE I
OPERATING CONDITIONS OF P&O ALGORITHM

	Condition		Action	
1	$I_{LRMS}(k)>I_{LRMS}(k\text{-}n)$	$D_1(k\text{-}1)>D_1(k\text{-}n)$ & $P_e(k)\leq P_{tol}$	Decrease D_1	$D_1(k)=D_1(k\text{-}n)\text{-}(\Delta D_1)_I$
2	$I_{LRMS}(k)<I_{LRMS}(k\text{-}n)$	$D_1(k\text{-}1)>D_1(k\text{-}n)$ & $P_e(k)\leq P_{tol}$	Increase D_1	$D_1(k)=D_1(k\text{-}n)\text{-}(\Delta D_1)_I$
3	$I_{LRMS}(k)>I_{LRMS}(k\text{-}n)$	$D_1(k\text{-}1)>D_1(k\text{-}n)$ & $P_e(k)>P_{tol}$	-Decrease D_1 -Fine tune D_1 to minimise P_e	$D_1(k)=D_1(k\text{-}n)\text{-}(\Delta D_1)_I$ $+(\Delta D_1)_P$
4	$I_{LRMS}(k)<I_{LRMS}(k\text{-}n)$	$D_1(k\text{-}1)>D_1(k\text{-}n)$ & $P_e(k)>P_{tol}$	-Increase D_1 -Fine tune D_1 to minimise P_e	$D_1(k)=D_1(k\text{-}n)\text{-}(\Delta D_1)_I$ $+(\Delta D_1)_P$
5	$I_{LRMS}(k)>I_{LRMS}(k\text{-}n)$	$D_1(k\text{-}1)<D_1(k\text{-}n)$ & $P_e(k)\leq P_{tol}$	Increase D_1	$D_1(k)=D_1(k\text{-}n)+(\Delta D_1)_I$
6	$I_{LRMS}(k)<I_{LRMS}(k\text{-}n)$	$D_1(k\text{-}1)<D_1(k\text{-}n)$ & $P_e(k)\leq P_{tol}$	Decrease D_1	$D_1(k)=D_1(k\text{-}n)+(\Delta D_1)_I$
7	$I_{LRMS}(k)>I_{LRMS}(k\text{-}n)$	$D_1(k\text{-}1)<D_1(k\text{-}n)$ & $P_e(k)>P_{tol}$	-Increase D_1 -Fine tune D_1 to minimise P_e	$D_1(k)=D_1(k\text{-}n)+(\Delta D_1)_I$ $+(\Delta D_1)_P$
8	$I_{LRMS}(k)<I_{LRMS}(k\text{-}n)$	$D_1(k\text{-}1)<D_1(k\text{-}n)$ & $P_e(k)>P_{tol}$	-Decrease D_1 -Fine tune D_1 to minimise P_e	$D_1(k)=D_1(k\text{-}n)+(\Delta D_1)_I$ $+(\Delta D_1)_P$

IV. CLOSED LOOP CONTROL DESIGN

The power-flow closed loop control scheme is presented in this section to enable real time implementation of the proposed MCPT technique. Fig. 7 shows the proposed control scheme for the DAB converter. The proposed P&O algorithm is embedded in the control scheme to obtain optimum duty ratios (i.e.: achieve minimum AC link RMS current.). The control scheme is generalised for DAB converter regardless of power and voltage ratings. In addition, it incorporates all possible operating modes of the dual active bridge converter, namely: unity gain mode ($K_{12}=1$) and Buck/boost modes ($K_{12}\neq 1$). In unity gain mode there is no need to apply the MCPT technique as the minimum current in this case is obtained at unity duty ratios (D_1=D_2=1), which achieve equal RMS bridge voltages while keeping minimum RMS current [15]. At buck/boost operating mode, the MCPT technique is utilised to obtain optimal modulation parameters (D_1, D_2). Moreover, phase shift (D_{12}) is obtained via a conventional PI controller in order to control power flow. Associated implementation steps are described as follows:

1) Read P and P^*;
2) PI controller regulates phase shift D_{12} to track P^* (continuous step);
3) Read P, P^*, $I_{L\,RMS}$, V_{dc1} and V_{dc2} and calculate DC voltage ratio K_{12}:
   a. If K_{12} is not unity then apply MCPT technique (perturb calculation and P&O) as depicted in Fig. 6. First iteration of P&O employs D_1=1 and second iteration employs an initial small perturb $(\Delta D_1)_I$;
   b. If K_{12} is unity then D_1=D_2=1 [15];
4) D_1 and D_2 are updated and sent to TPS modulator. Then repeat steps 1-4.

V. SIMULATION RESULTS

The proposed MCPT technique is applied on a detailed switching DAB converter in Matlab/Simulink for validation. Achieved RMS current are benchmarked with the minimum RMS current obtained using the PSO-based method in [15] to verify that minimum current is obtained. The simulations were carried out using the DAB parameters described in Table II. Simulation results for two case studies are presented in Fig. 8 and Fig. 9, thus highlighting the performance of the DAB converter under the proposed controller. Fig.8(a) and Fig.9(a) show that the controller satisfies the required P^*. Fig.8(g) and Fig.9(b) show the actual RMS current along with minimum RMS current. The relative difference at the beginning of the perturbation is high as unity duty ratios are employed. Then this difference starts to decrease as the P&O moves the operating point of the DAB converter toward the optimal TPS ratios achieving minimum RMS current with negligible oscillations in steady state. Fig.8(f) shows that the operation starts at D_1=1 & D_2=1, then the perturbs are applied to D_1 until minimum current point is achieved at steady state. For each value of D_1, D_2 is calculated via (5) and D_{12} is calculated via PI controller to meet reference power. The value of D_1 is oscillation-free at steady state as well as the power transferred and AC link RMS current waveforms, this is thanks to the proposed adaptive-step PI-based calculation method discussed in detail in sections (III-B) and (III-C). The changes applied to the TPS ratios are also reflected via the corresponding AC side waveforms v_p, v_s and i_L shown in Fig. 8 (b)-(e).

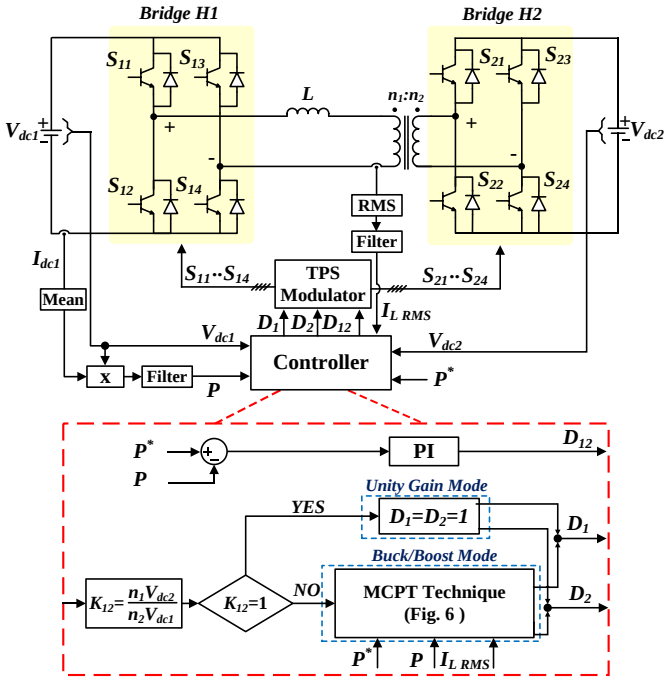

Fig. 7: Proposed MCPT power-flow control scheme for DAB converter.

TABLE II
PARAMETERS OF DAB CONVERTER IN SIMULATION

Parameter	value
Bridge 1 DC Voltage V_{dc1}	100V
Bridge 2 DC Voltage V_{dc2}	40V (K_{12}=0.4) 50V (K_{12}=0.5) 60V (K_{12}=0.6)
Switching Frequency f_s	2.5kHz
Base Power P_{base}	500W
Equivalent AC link inductance L	1mH

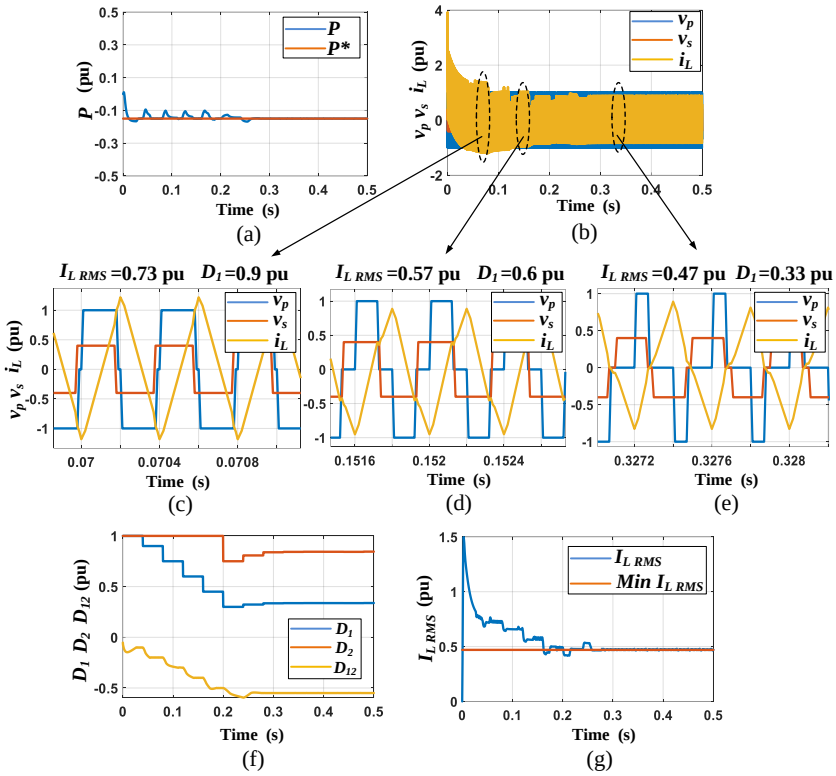

Fig 8: Steady state perfromance of DAB Converter under proposed MCPT controller at K_{12}=0.4 and P*=-0.15pu : (a)Transferred Power. (b)-(e)AC side waveforms. (f)TPS ratios. (g)AC Link's RMS current.

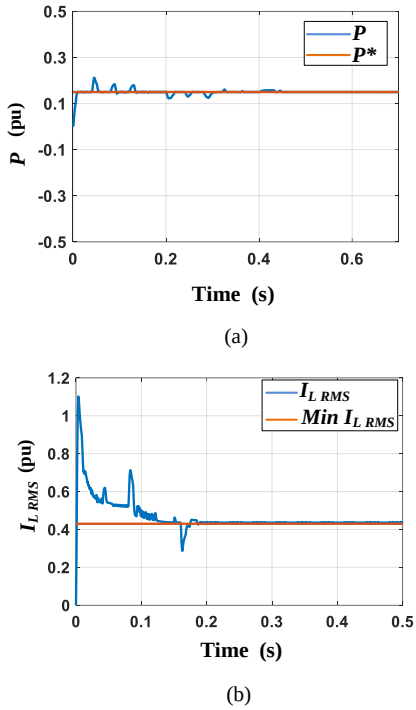

Fig 9: Steady state perfromance of DAB Converter under proposed MCPT controller at K_{12}=0.6 and P*=0.2pu: (a)Transferred Power. (b) AC Link's RMS current.

In addition, to validate the robustness of the controller to different system parameters, a simulation was carried out with different value of AC Link equivalent inductance (L=3mH). Results are shown in Fig.10 showing that the controller performance is not dependent on circuit parameters. Furthermore, to demonstrate the dynamic response of the controller, a simulation including step change in reference power (value and direction of reference power) is shown in Fig.11. The changes applied to D_1 (the perturbation parameter) due to P&O algorithm along with the other TPS ratios D_2 and D_{12} are shown in Fig.11 (f). At the instant of the step change in reference power, the controller resets and start perturbing at D_1=1 until the minimum current point (MCP) is reached while maintaining the required power level. It can be noticed that the second case (P*=0.31) the MCP is reached in a relatively lower transient time (compared to first case from t=0.0 to 0.6 sec). That is because at P*=0.31pu the optimal modulation parameters are at D_1=0.85 & D_2=1 and the perturbation always initiates at D_1=1 which explains the corresponding lower transient time compared to the first case. The effect of the online adjustments of TPS ratios is also demonstrated in the AC side waveforms v_p, v_s and i_L shown in Fig.11(b)-(e). The reason for the ripples in the transferred power waveforms shown in Figs. 8,9 and 10 part (a) – during the transient stage – is that after each perturbation (online iteration) the duty ratios (D_1, D_2) change hence the PI-controller change phase shifts (D_{12}) to maintain the required power levels (P^*).

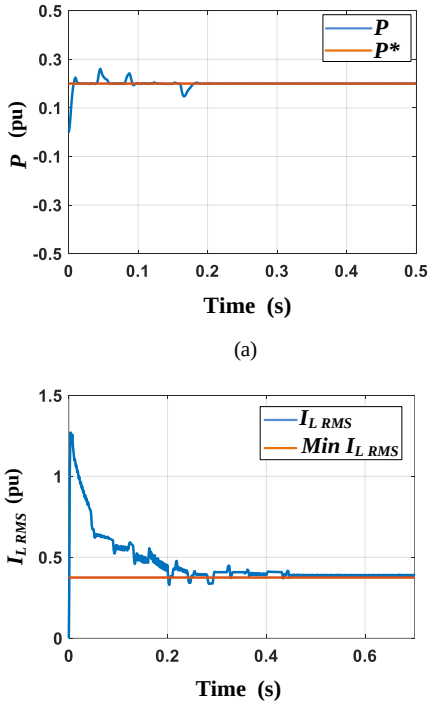

Fig 10: Robustness of proposed MCPT controller with different system parameters at K_{12}=0.5 and P*=0.15pu: (a)Transferred Power. (b) AC Link's RMS current.

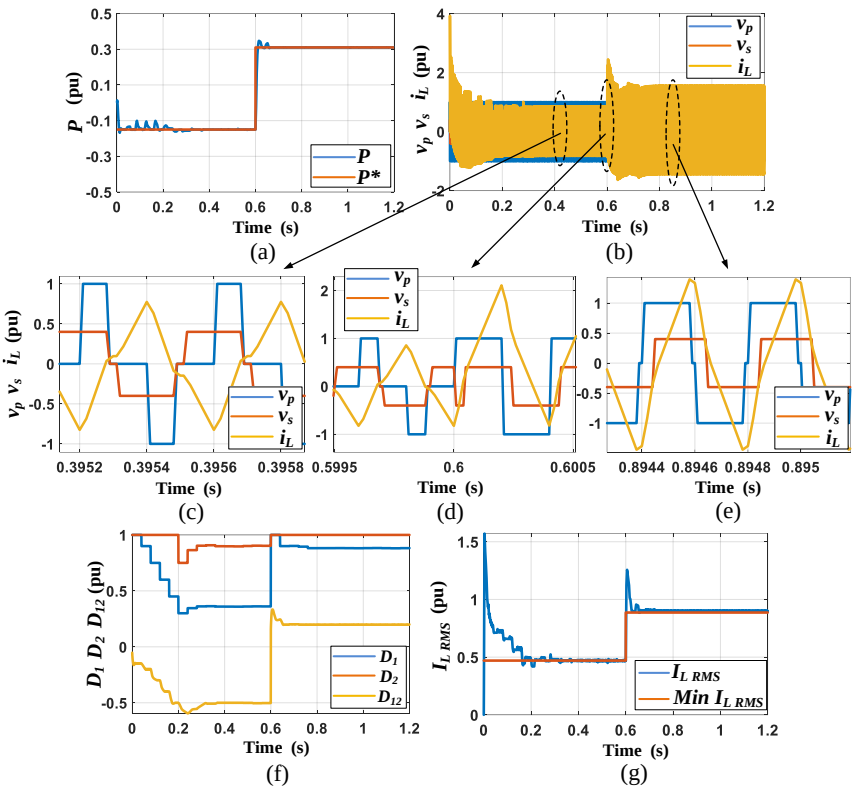

Fig 11: Dynamic Perfromance of DAB Converter under proposed MCPT controller with reference power change in value and direction at K_{12}=0.4 and P*=-0.15, 0.31 pu: (a)Transferred Power. (b)-(e)AC side waveforms. (f)TPS ratios. (g)AC Link's RMS current.

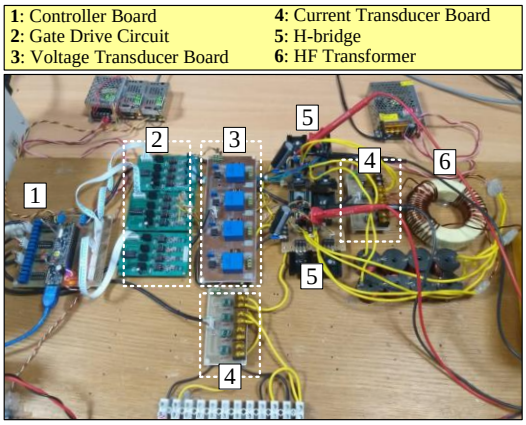

Fig. 12: Experimental test rig for DAB.

TABLE III.
PARAMETERS OF EXPERIMENTAL DAB CONVERTER

Parameter	value
Bridge 1 DC Voltage V_{dc1}	100V
Bridge 2 DC Voltage V_{dc2}	20V (K_{12}=0.4) 30V (K_{12}=0.6)
Transformer turns ratio ($a=n_1/n_2$)	2
Switching Frequency f_s	2.5kHz
Base Power P_{base}	476W
Transformer total leakage inductance L *(referred to primary)*	1.05mH

VI. EXPERIMENTAL RESULTS

A low scaled experimental DAB setup is shown in Fig.12. This was developed according the schematic depicted in Fig. 7 in order to validate the proposed closed loop controller. The parameters used for designing the test rig are listed in Table III. Two programmable power supplies are used to represent the behaviour of the two DC sides, and the two active H-bridges are connected through a transformer. The semiconductor switches used are MOSFETs (MOSFET IRF250) while a CY8C5888LTI-LP097 PSoC 5LP microcontroller was used. The current and the voltage feedback for the controller is done by using Hall-effect current transducers.

The steady state performance before and after applying the proposed control scheme is depicted in Figs 13-15 at different operating points that represent different DC voltage mismatch (K_{12}) and different loading (P*). Figs 13-15 shows the AC side readings of the primary and secondary sides (v_p, v_s, i_p, i_s) plus the RMS current reading at both primary and secondary sides of transformer. The effectivness of the controller is clearly noted from the minimized RMS current and efficieny improvment before and after applying the proposed controller as shown in Figs 13-15.

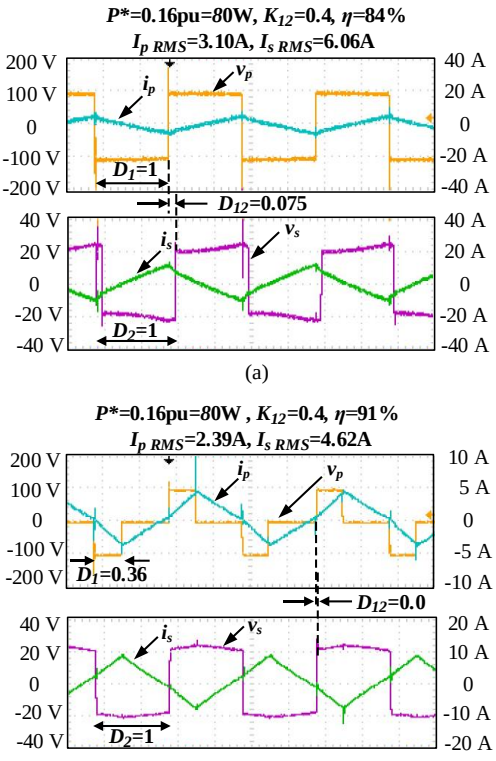

Fig 13: Steady State Perfromance of DAB Converter under proposed MCPT controller in exepriment at K_{12}=0.4 and P*=0.16pu (80W): (a)Before applying the proposed technique. (b) After applying the proposed technique.

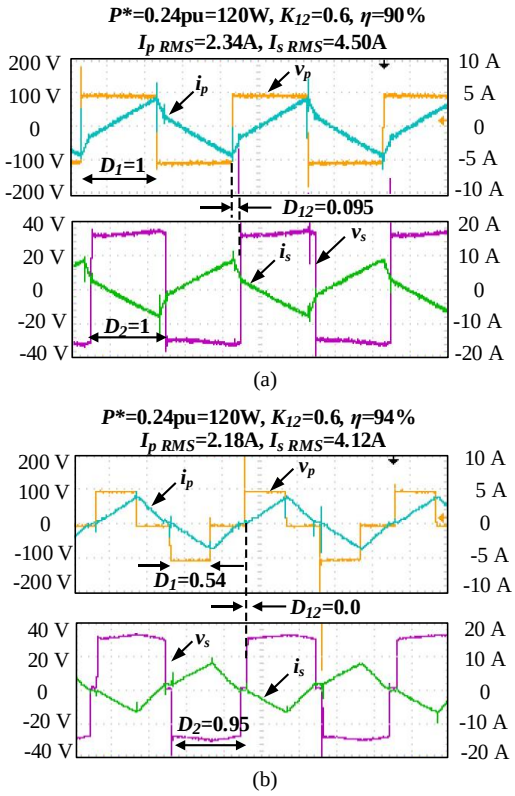

Fig 14: Steady State Perfromance of DAB Converter under proposed MCPT controller in exepriment at K_{12}=0.6 and P*=0.24pu(120W): (a)Before applying the proposed technique. (b) After applying the proposed technique.

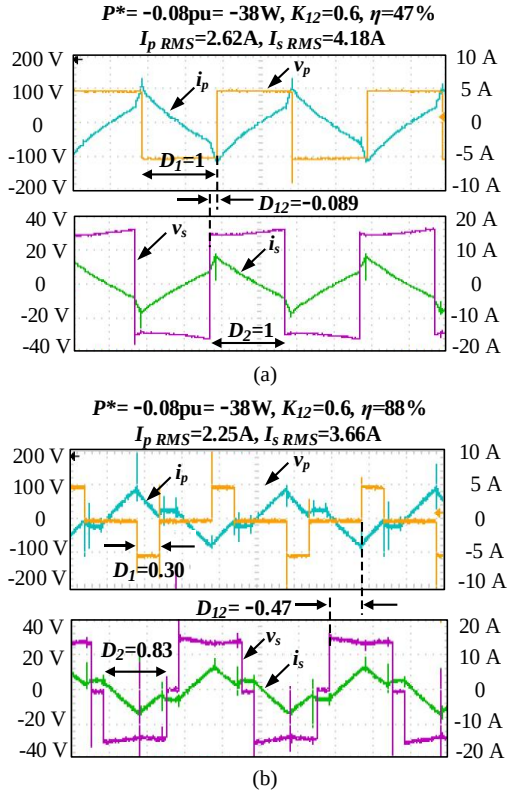

Fig 15: Steady State Perfromance of DAB Converter under proposed MCPT controller in exepriment at K_{12}=0.6 and P*=-0.08pu (-38W): (a)Before applying the proposed technique. (b) After applying the proposed technique.

For further verification of the effectiveness of the controller, comparative efficiency curves (between conventional phase shift (CPS) and the proposed controller) are presented in Fig.16 at many operating points representing different DC voltage mismatch (K_{12}) and different power levels (P*).

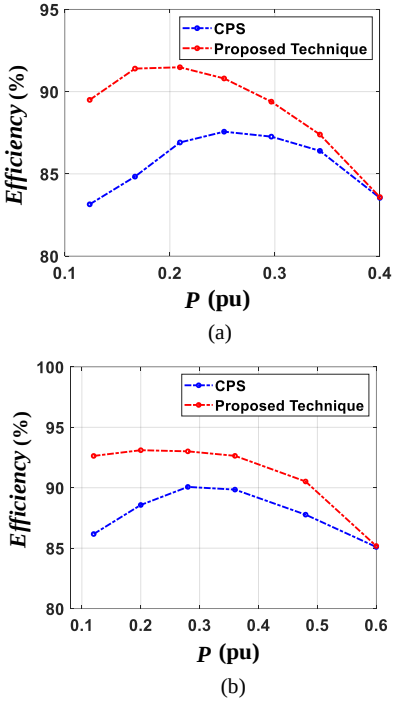

Fig 16: Efficiency curves in experiment using conventional phase shift (CPS) and the proposed controller:(a) K_{12}=0.4, (b) K_{12}=0.6.

VII. Conclusion

A power regulation controller for dual active bridge DC−DC converter based on a new scheme that tracks minimum RMS current to ensure minimum losses has been proposed. The DAB I-V characteristic revealed the existence of a global minimum current for every level of active power transferred between the DC sides. This minimum current point can be tracked based on a P&O algorithm and combined with a closed loop controller to regulate power to desired level. The proposed controller is generic and, unlike existing efforts in this area, is independent of circuit parameters and is not derived from complex converter modeling. Extensive simulations and an experimental test rig verified the effectiveness and potential of the proposed scheme. Future research points for the current work may involve transient time minimisation to improve the controller response.

References

[1] W. R. Leon Garcia, P. Tixador, B. Raison, A. Bertinato, B. Luscan, and C. Creusot, “Technical and Economic Analysis of the R-Type SFCL for HVDC Grids Protection,” *IEEE Trans. Appl. Supercond.*, vol. 27, no. 7, 2017.

[2] B. Zhao, Q. Song, J. Li, Q. Sun, and W. Liu, “Full-Process Operation, Control, and Experiments of Modular High-Frequency-Link DC Transformer Based on Dual Active Bridge for Flexible MVDC Distribution: A Practical Tutorial,” *IEEE Trans. Power Electron.*, vol. 32, no. 9, pp. 6751–6766, 2017.

[3] A. Nisar and M. S. Thomas, “Comprehensive Control for Microgrid Autonomous Operation with Demand Response,” *IEEE Trans. Smart Grid*, vol. 8, no. 5, pp. 2081–2089, 2017.

[4] D. Sha, X. Wang, and D. Chen, “High-Efficiency Current-Fed Dual Active Bridge DC-DC Converter With ZVS Achievement Throughout

Full Range of Load Using Optimized Switching Patterns," *IEEE Trans. Power Electron.*, vol. 33, no. 2, pp. 1347–1357, 2018.
[5] A. Tong, L. Hang, G. Li, X. Jiang, and S. Gao, "Modeling and Analysis of a Dual-Active-Bridge-Isolated Bidirectional DC / DC Converter to Minimize RMS Current With Whole Operating Range," *IEEE Trans. Power Electron.*, vol. 33, no. 6, pp. 5302–5316, 2018.
[6] L. Yuan, Z. Zhao, J. Sun, J. Nie, and Q. Gu, "Current Stress Minimization of Dual Active Bridge DC-DC Converter within the Whole Operating Range," *IEEE J. Emerg. Sel. Top. Power Electron.*, vol. 7, no. 1, pp. 1–1, 2018.
[7] H. Wen, W. Xiao, and B. Su, "Nonactive power loss minimization in a bidirectional isolated DC-DC converter for distributed power systems," *IEEE Trans. Ind. Electron.*, vol. 61, no. 12, pp. 6822–6831, 2014.
[8] Y. A. Harrye, K. H. Ahmed, and A. A. Aboushady, "Reactive power minimization of dual active bridge DC/DC converter with triple phase shift control using neural network," *3rd Int. Conf. Renew. Energy Res. Appl. ICRERA 2014*, pp. 566–571, 2014.
[9] H. Shi, H. Wen, Y. Hu, and L. Jiang, "Reactive Power Minimization in Bidirectional DC-DC Converters Using a Unified-Phasor-Based Particle Swarm Optimization," *IEEE Trans. Power Electron.*, vol. 33, no. 12, pp. 10990–11006, 2018.
[10] B. Zhao, Q. Yu, and W. Sun, "Extended-phase-shift control of isolated bidirectional DC-DC converter for power distribution in microgrid," *IEEE Trans. Power Electron.*, vol. 27, no. 11, pp. 4667–4680, 2012.
[11] J. Huang, Y. Wang, Z. Li, and W. Lei, "Unified Triple-Phase-Shift Control to Minimize Current Stress and Achieve Full Soft-Switching of Isolated Bidirectional DC-DC Converter," *IEEE Trans. Ind. Electron.*, vol. 63, no. 7, pp. 4169–4179, 2016.
[12] N. Hou, W. Song, and M. Wu, "Minimum-Current-Stress Scheme of Dual Active Bridge DC-DC Converter with Unified Phase-Shift Control," *IEEE Trans. Power Electron.*, vol. 31, no. 12, pp. 8552–8561, 2016.
[13] B. Zhao, Q. Song, W. Liu, and W. Sun, "Current-stress-optimized switching strategy of isolated bidirectional DC-DC converter with dual-phase-shift control," *IEEE Trans. Ind. Electron.*, vol. 60, no. 10, pp. 4458–4467, 2013.
[14] F. Krismer and J. W. Kolar, "Closed form solution for minimum conduction loss modulation of DAB converters," *IEEE Trans. Power Electron.*, vol. 27, no. 1, pp. 174–188, 2012.
[15] O. M. Hebala, A. A. Aboushady, K. H. Ahmed, and I. Abdelsalam, "Generic Closed-Loop Controller for Power Regulation in Dual Active Bridge DC-DC Converter With Current Stress Minimization," *IEEE Trans. Ind. Electron.*, vol. 66, no. 6, pp. 4468–4478, 2019.
[16] G. Ortiz, H. Uemura, D. Bortis, J. W. Kolar, and O. Apeldoorn, "Modeling of soft-switching losses of IGBTs in high-power high-efficiency dual-active-bridge DC/DC converters," *IEEE Trans. Electron Devices*, vol. 60, no. 2, pp. 587–597, 2013.
[17] F. Xue, R. Yu, and A. Q. Huang, "A 98.3% Efficient GaN Isolated Bidirectional DC-DC Converter for DC Microgrid Energy Storage System Applications," *IEEE Trans. Ind. Electron.*, vol. 64, no. 11, pp. 9094–9103, 2017.
[18] N. Femia, G. Lisi, G. Petrone, G. Spagnuolo, and M. Vitelli, "Distributed Maximum Power Point Tracking of Photovoltaic Arrays : Novel Approach and System Analysis," vol. 55, no. 7, pp. 2610–2621, 2008.
[19] M. Fortunato, A. Giustiniani, G. Petrone, G. Spagnuolo, and M. Vitelli, "Maximum Power Point Tracking in a Photovoltaic Inverter," *IEEE Trans. Ind. Electron.*, vol. 55, no. 7, pp. 2684–2693, 2008.
[20] S. Park, G. Cha, Y. Jung, C. Won, and S. Member, "Design and Application for PV Generation System Using a Soft-Switching Boost Converter With SARC," *IEEE Trans. Ind. Electron.*, vol. 57, no. 2, pp. 515–522, 2010.
[21] M. A. Elgendy, B. Zahawi, and D. J. Atkinson, "Assessment of perturb and observe MPPT algorithm implementation techniques for PV pumping applications," *IEEE Trans. Sustain. Energy*, vol. 3, no. 1, pp. 21–33, 2012.
[22] A. K. Abdelsalam, A. M. Massoud, S. Ahmed, and P. N. Enjeti, "High-performance adaptive Perturb and observe MPPT technique for photovoltaic-based microgrids," *IEEE Trans. Power Electron.*, vol. 26, no. 4, pp. 1010–1021, 2011.

Osama M. Hebala received the B.Sc. (Hons.) and M.Sc. degrees in Electrical and Control Engineering from Arab Academy for Science, Technology & Maritime Transport (AASTMT), Alexandria, Egypt, in 2011 and 2015, respectively. He received the Ph.D. degree in power electronics from Robert Gordon University, Aberdeen, UK, 2020. Currently he is a lecturer in Electric & Control Engineering department at Arab Academy for Science, Technology and Maritime Transport, Alexandria, Egypt. His research interests include DC–DC converters, power conversion systems, and power systems planning and optimization.

Ahmed A. Aboushady (M'04, SM'17) received his BSc (Hons) and MSc degrees in Electrical and Control Engineering from the Arab Academy for Science and Technology, Egypt in 2005 and 2008 respectively. Following this, he obtained his PhD degree in power electronics form the University of Strathclyde, UK in 2013. He is currently a Senior Lecturer in power electronic systems at Glasgow Caledonian University, UK. Dr Aboushady has several publications in refereed journals/conferences as well as a published textbook, a book chapter contribution and a PCT patent No. PCT/GB2017/051364. His research interests are DC/DC converters, high voltage DC transmission systems, grid integration of renewable energy and distributed generation systems.

Khaled H. Ahmed (M'09, SM'12) received the B.Sc. (Hons.) and M.Sc. degrees from Alexandria University, Egypt in 2002 and 2004, respectively. He received the Ph.D. degree in power electronics applications from the University of Strathclyde, UK, 2008. He was appointed as a Professor at Alexandria University, Egypt since 2019. Currently, Dr Ahmed is a Reader in Power Electronics at the University of Strathclyde, UK. He is a senior member of the IEEE Power Electronics and Industrial Electronics societies. Dr Ahmed has published more than 100 technical papers in refereed journals and conferences as well as a published textbook entitled 'High Voltage Direct Current Transmission: Converters, Systems and DC Grids', a book chapter contribution, and a PCT patent PCT/GB2017/051364. His research interests are renewable energy integration, high power converters, offshore wind energy, DC/DC converters, HVDC, and smart grids.

Ibrahim Abdelsalam received a first class B.Sc. and M.Sc. degrees in Electrical Engineering from the Arab Academy for Science and Technology and Maritime Transport (AASTMT), Egypt, in 2006(Alexandria campus) and 2009(Cairo campus). He received the Ph.D. degree in power electronics from University of Strathclyde, Glasgow, UK, 2016. Currently he is a lecturer in Electrical Engineering Department at Arab Academy for Science, Technology and Maritime Transport. His research interests are power electronic converters and their applications in wind energy conversion systems, and advanced control strategies of the multilevel voltage and current source converters.

Samuel J. Burgess was born in Northern Ireland, U.K. He received a B.Eng. (Hons) Degree in Electronic Systems and a D.Phil. degree in radio frequency studies from the University of Ulster, Jordanstown, U.K., in 1996 and 1999, respectively. From 2000 to 2003, he worked in the Radio Frequency group of Parthus Technologies (Ireland) as a Project Engineer on the design of sub-micron CMOS circuits for wireless applications. From late 2003 to 2014 he was a lecturer at the University of Ulster in the area of electronics and communications. Since late 2014 he has been with Robert Gordon University, Aberdeen, Scotland, U.K., where he is currently an Academic Strategic Lead and Head of Electronic & Electrical studies in the School of Engineering. Dr Burgess has 17 years University experience and 9 years industrial experience. His teaching and research interests include radio frequency design, control systems, wireless communications, analogue electronics and sensor systems.